

Modelling Seismic Data for Time-varying Rough Sea Surfaces

E. Cecconello* (EOST), E. G. Asgedom (PGS Geophysical AS), O.C. Orji (PGS Geophysical AS) & W. Söllner (PGS Geophysical AS)

SUMMARY

The impact of moving rough sea surfaces on seismic data can only be assessed through proper modelling. Existing seismic data modelling tools assume either flat or frozen sea surfaces. We present a tool for modelling seismic data from a time-varying rough sea surfaces. This is achieved by coupling the up-going subsurface reflection data with the time-varying sea surface reflectivity on a plane interface below the sea surface using integral technique. The algorithm was verified with known analytical solutions for both frozen and moving sea surfaces. Our data examples show that time varying sea surfaces affect reflection signals significantly in comparison to the static counterpart.

Introduction

Understanding the effects of moving rough sea surfaces on seismic data is crucial to the advancing of broadband seismic technologies. Modelling sea surface effects on seismic wavefield using either Ray-Tracing or Finite-Difference is not well suited due to the intrinsic limitations of these methods. Here, we derived an acoustic reciprocity based integral method and employed this to couple the up-going subsurface reflection data with the time-varying sea surface reflectivity on a plane interface below the sea surface. The time-varying sea surface reflectivity was computed by deriving a similar integral equation with connecting interface at the sea surface. This method for computing the receiver ghost is verified by comparing with known analytical solutions for both frozen and moving sea surfaces. Finally, results for realistic time-varying sea surfaces are presented.

Method

The receiver ghost pressure wavefield for time-varying sea surfaces is derived based on Rayleigh's reciprocity theorem in time domain as schematically shown in Figure 1. In state A, the up-going subsurface reflected pressure gradient, ∇p^{A-} is modelled while the sea surface reflectivity p^{B+} is modelled in state B. Finally, the receiver ghost, p^{A+} , including both subsurface and sea surface information, is obtained by coupling the two states at the connecting level, S_0 , below the sea surface.

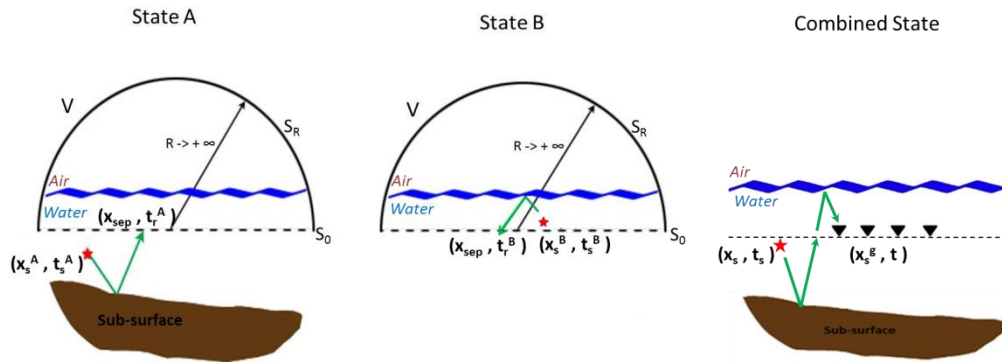


Figure 1 States A and B are coupled to generate the receiver ghost.

Mathematically, this is written as:

$$p^{A+}(x_s^g, t; x_s, t_s) = -\frac{2}{\rho} \int_{-\infty}^{+\infty} \int_{S_0} p^{B+}(x_{sep}, t - t_r^A; x_s^g, 0) \nabla p^{A-}(x_{sep}, t_r^A; x_s, t_s) dS_0 dt_r^A \quad (1)$$

The sea surface reflectivity is then derived using the same principle as explained above with connecting level now at the sea surface. This is represented by decomposing state B into states C and D as shown in Figure 2.

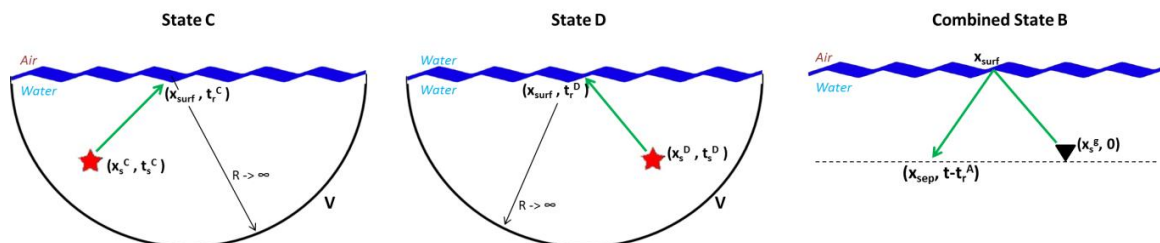


Figure 2 State C and D are coupled to generate the sea surface reflectivity wavefield.

Mathematically, this is given by:

$$p^{B+}(\mathbf{x}_{sep}, t - t_r^A; \mathbf{x}_s^g, 0) = \frac{1}{\rho} \int_{-\infty}^{+\infty} \int_{S_f(t_r^C)} p^D(\mathbf{x}_{surf}, t - t_r^A - t_r^C; \mathbf{x}_{sep}, 0) \nabla p^C(\mathbf{x}_{surf}, t_r^C; \mathbf{x}_s^g, 0) d\mathbf{S}_f(t_r^C) dt_r^C \quad (2)$$

State C represents the pressure gradient, ∇p^C , with sources at the separation level and receivers at the free surface. This is computed using integral inversion or alternatively by Kirchhoff approximation (Thorsos, 1988; Orji et al., 2012). These two implementations are benchmarked against each other in the next section. State D represents the pressure wavefield, p^D , with sources at the receiver level and receivers at the sea surface.

Replacing p^{B+} in Equation (1) by Equation (2), we obtain the Varying Boundary Wavefield Modeling method (VBWM):

$$p^{A+}(\mathbf{x}_s^g, t; \mathbf{x}_s, t_s) = \frac{2}{\rho^2} \int_{-\infty}^{+\infty} \int_{S_0} \int_{-\infty}^{+\infty} \int_{S_f(t_r^C)} p^D(\mathbf{x}_{surf}, t - t_r^A - t_r^C; \mathbf{x}_{sep}, 0) \nabla p^C(\mathbf{x}_{surf}, t_r^C; \mathbf{x}_s^g, 0) \nabla p^{A+}(\mathbf{x}_{sep}, t_r^A; \mathbf{x}_s, t_s) d\mathbf{S}_f(t_r^C) dt_r^C d\mathbf{S}_0 dt_r^A \quad (3)$$

Verification and Benchmarking – Stationary sea surface

To quality control our synthetic data, the receiver ghost is first computed (using Equation (3)) for a stationary flat sea surface and a flat subsurface reflector and verified against the analytical solution for a flat sea (i.e. using mirror method). The results show very good match. Edge effects as a result of integration were removed by padding and tapering.

A similar simulation is repeated for a frozen rough sea surface generated based on Pierson-Moskowitz spectrum with a wind speed of 15m/s (Pierson and Moskowitz, 1963). The sea state has a significant wave height of 4.8m and dominant wavelength of 203m. In Figure 3, the left plot shows the VBWM result using Kirchhoff approximation to generate the sea surface reflectivity wavefield, the middle plot shows the VBWM result using the integral inversion for the sea surface reflectivity, and the right plot shows the difference between the two. Integral inversion correctly predicts incoherent scattering and whilst Kirchhoff approximation does not, the error is shown to be small for this case. Since Kirchhoff approximation is much less computationally demanding it was selected for the next steps in this work.

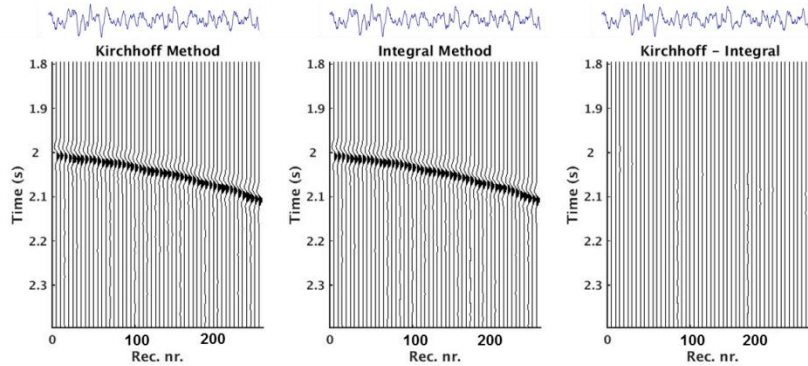


Figure 3 Results for a rough sea surface using VBWM with Kirchhoff approximation (left), VBWM with Integral method (middle) and the difference (right). The rough sea is indicated on top of all the plots.

Verification – Moving flat sea surface

Data was computed for a flat sea surface moving upward (away from the stationary source and receivers) with a velocity of 300m/s, and the same surface moving downward (toward the source and

receiver) with the same speed and for the stationary surface. The three cases are benchmarked to the analytically modelled data (Cooper, 1980). The purpose of this exercise was to further verify the method and its implementation. The data computation configuration here does not represent any physically realistic case.

The VBWM method correctly predicts the expected Doppler frequency shift and the amplitude changes. In Figure 4, the blue curve corresponds to the sea surface moving upward, the red curve is the stationary case, the black curve corresponds to the sea surface moving downward and the magenta stars are the analytically derived amplitude values.

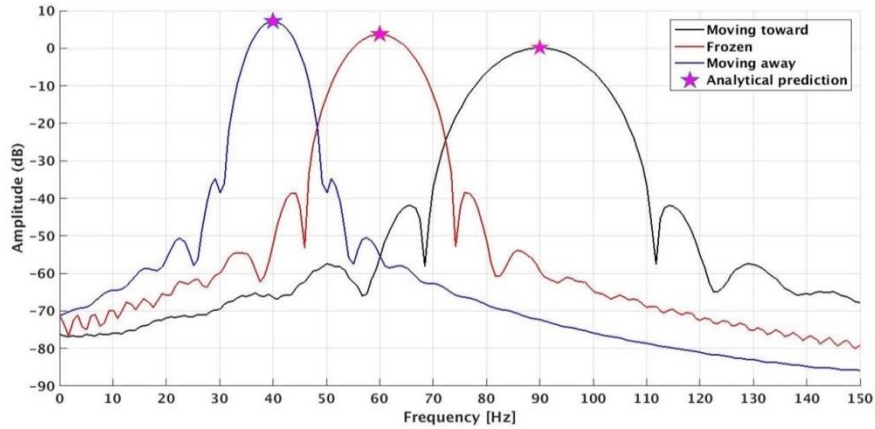


Figure 4 Doppler shifts in frequency and amplitude.

Time-varying rough sea surface results

Finally, the receiver ghost is computed for a model consisting of a time-varying rough sea surface (Figure 5B) and a dipping plane layer subsurface (with configuration as displayed in Figure 5A). Figure 5B shows the time evolution of the sea surface elevation the rectangular windows highlight three recording times where data for the time-varying sea surfaces are computed. These results are compared to the result from the frozen sea surface (Figure 5C), using the rough sea surface realization at time zero in Figure 5B. In Figure 6, we present the results of the VBWM method for the three shots: The left plot represents the shot gather recorded from 0s to 0.6s (red window), the middle plot represents the shot gather recorded from 10s to 10.6s (green window) and the right plot represents the shot gather from 20s to 20.6s (blue window). In Figure 7, the differences to the frozen case (Figure 5C) are displayed. A t^2 amplitude correction has been applied for visualization purposes. The plots show clearly that as the sea surface evolves, the difference between the data computed from the stationary sea surface and that from the time varying sea surface increases significantly.

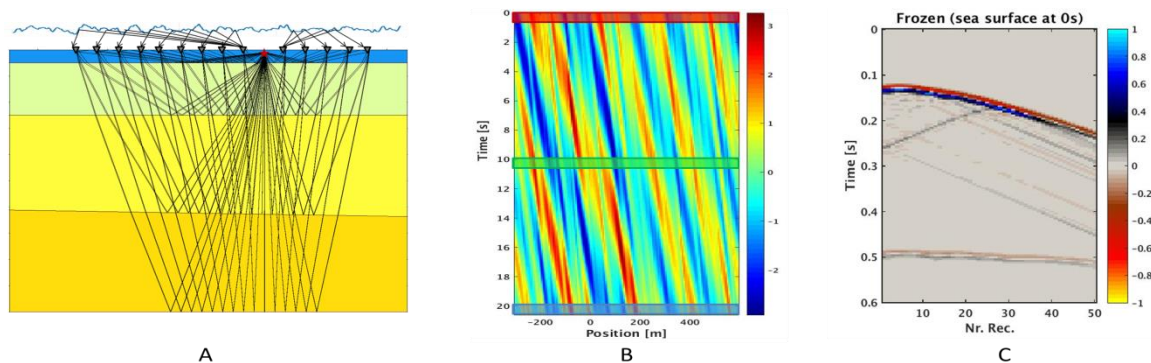


Figure 5 A - Synthetic data Computation configuration. B -Variation of the sea surface elevation with time, the red rectangle highlight the recording time of the first shot, the green rectangle that of

the second shot and the blue rectangle that of the third shot. C – Shot gather computed assuming a stationary rough sea surface generated at 0s of Figure 5B.

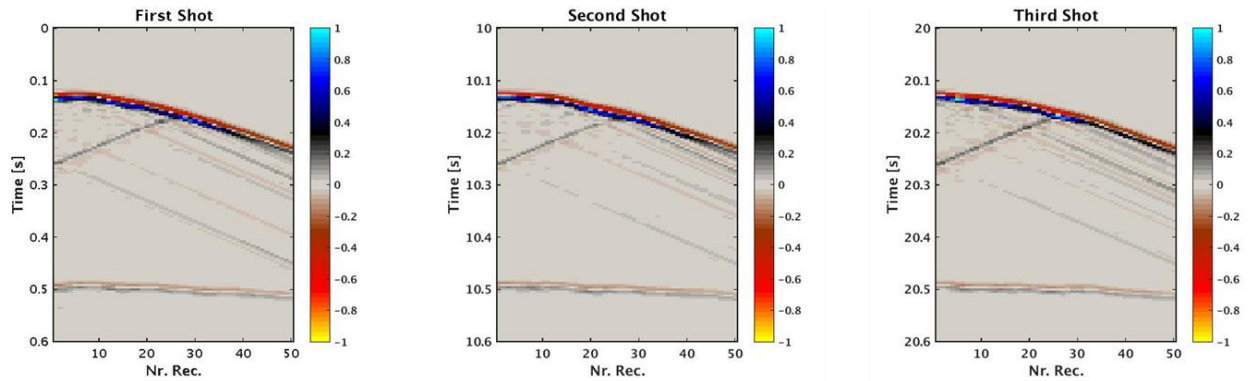


Figure 6 Shot records computed with VBWM – Kirchhoff approximation and a time-varying rough sea surface from 0s to 0.6s (left panel), from 10s to 10.6s (middle panel), and from 20s to 20.6s (third panel).

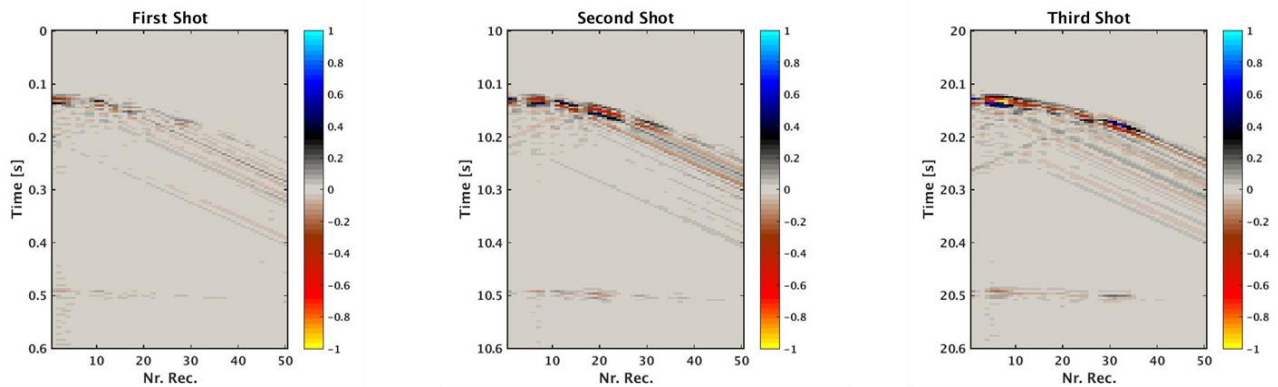


Figure 7 Difference between the shot gather considering a stationary sea surface generated at 0s (see Figure 5C) and that of a time-varying rough sea surface moving from 0s to 0.6s (left panel), from 10s to 10.6s (middle panel), and from 20s to 20.6s (third panel).

Conclusion

We have developed a method for time-varying rough sea surface wavefield modelling. This method has been verified by analytical solutions for a moving flat sea surface. Our modelling results highlight the fact that the interaction with a realistic time-varying rough sea surface affects the subsurface reflection signals to a larger degree than a static rough sea surface and can be seen to further compromise the interpretability of the seismic events.

References

- Cooper, J. [1980] Scattering of electromagnetic fields by a moving boundary: the one dimensional cases. *Antennas and Propagation, IEEE Transactions on*, **28**(60), 791-795.
- Orji, O. C., Söllner W., and Gelius, L.-J. [2012] Effects of time-varying sea surface in marine seismic data. *Geophysics*, **77**(3), P33-P43.
- Pierson Jr, W. J. and Moskowitz, L. [1963] A proposed spectral form for fully developed wind seas based on the similarity theory of S.A. Kitaigorodskii. Technical report, DTIC Document.
- Thorsos, E. I. [1988] The validity of the Kirchhoff approximation for rough surface scattering using a gaussian roughness spectrum. *The Journal of the Acoustical Society of America*, **83**(1), 78-92.